EPJ Web of Conferences **6**, 16002 (2010)
DOI:10.1051/epjconf/20100616002

DIC-aided biaxial fatigue tests of a 304L steel

M. Poncelet[1,a], G. Barbier[2,3], B. Raka[2], S. Courtin[4], R. Desmorat[2], J.C. Le-Roux[3], and L. Vincent[1]

[1] CEA Saclay, DEN, SRMA, 91191 Gif-sur-Yvette cedex, France
[2] LMT Cachan, 61 av. du Président Wilson, 94230 Cachan, France
[3] EDF R&D / MMC, Avenue des renardières – Ecuelles, 77818 Moret Sur Loing, France
[4] AREVA NP SAS, Tour AREVA, 92084 Paris La Défense, France

Abstract. Several biaxial fatigue tests are conducted up to 10^6 cycles at room temperature in the context of a collaboration LMT-Cachan / EDF / AREVA / SNECMA / CEA. Malteses cross specimens of 304L steel, designed to initiate crack in the bulk, are loaded by a triaxial testing machine. A Digital Image Correlation technique is used to measure strain during loading and detect crack initiation early. A special optical assembly and a stroboscopic sampling method are set up in this purpose. Several types of loadings are performed: equibiaxial with a loading ratio R = 0.1, equibiaxial with loading ratio R = –1, pseudo uniaxial (cyclic loading at R= 0.1 in one direction and constant loading in the other). First results are commented.

1 Introduction

Some parts of the cooling circuits of nuclear power plants are subject to high thermomechanical fluctuations because of the turbulent mixings of water at different temperatures. This may lead to thermal fatigue phenomena and the appearance of thermal cracking on the inner surface of tubes [1]. This phenomenon is the subject of numerous studies, from the understanding of thermomechanical loading to the prediction of structure failure. Because of the complex thermomechanical state, the experimental study of material behaviour under such loading is especially challenging. A first approach consists in reproducing the real thermomechanical loadings as accurately as possible [2], whereas the other consists in loading the samples mechanically in order to reproduce the typical stress states due to thermal loading. This second method is justified by the fact that the rather low temperature variation has little influence on High Cycle Fatigue (HCF) behavior [3]. Isothermal studies of the material can thus be conducted, far simplier experiments indeed. Moreover the mechanical loading induced by thermohydraulic solicitations in these parts of the circuits are now enough known to allow purely mechanical tests on specimens. Roughly speaking, they are multiaxial, with random patterns and non-zero mean stress.

A large partnership between LMT-Cachan / EDF / AREVA / SNECMA / CEA is behind the present study. The multiaxial HCF behavior is investigated through a dozen of tests performed on cross-specimens at room temperature.

[a] e-mail : martin.poncelet@cea.fr

The first difficulty of this study is linked to the material itself. The 304L austenitic stainless steel is indeed elasto-plastic in the HCF regime and the cyclic behavior never reaches a stabilized state. Moreover, this material is viscous at room temperature. The modeling of such alloys is thus not obvious in the uniaxial case, and even more so in multiaxial ones.

The multiaxial fatigue tests without measurement of the local loading, currently used in purely elastic cases, are pointless in the present case. Consequently one proposes an experimental protocol including strain field measurements to determine the applied strains in the gauge zone during cyclic loading. It is then possible to quantify the loading in terms of the evolution of the strain amplitude with the number of cycles, and to compare these results with uniaxial HCF ones if an equivalent strain is chosen. The detection of crack initiation is also performed thanks to full-field strain measurements to assess test stop instead of standard specimen failure criterion. In order to get the maximum of information from each test, an in-situ micrographic device is also used. Eventually, the experimental campaign is also used to identify a damage model (DAMAGE2005) [4] and to better understand/model the multiaxial cyclic behavior of 304L steels.

2 EXPERIMENTAL PROTOCOL

1.1 Studied material

The material used is a 304L steel produced by Creusot Loire Industrie. Its chemical composition is given in Table 1. The amount of residual ferrite measured by ferritscope is less than 1%, which is in good agreement with micrographic observations.

The mechanical properties under monotonic tension are given in Table 2. This steel is characterized by an important ratchetting phenomenon when non-zero mean stress cyclic loadings are applied (for more information, similar results are obtained for a 316L steel [5]). Moreover its cyclic behavior is never stabilized: first comes a cyclic softening and then a secondary hardening if the number of cycles to failure is high enough ([6]).

Table 1. Chemical composition of the 304L steel used (wt%).

C	Mn	Si	S	P	Ni	Cr	Mo	Cu	N_2
0.029	1.86	0.37	0.004	0.029	10.00	18.00	0.04	0.02	0.056

Table 2. Mechanical properties of the 304L steel used in the rolling direction at 20°C.

Yield stress $Y_{s0,2\%}$ (MPa)	Ultimate tesile stress UTS (MPa)	Elongation at failure A(%)	Young's modulus E (GPa)	Necking Z (%)
220	555	68	196	78

1.2 Specimens

Cross specimens (Figure 1 a) are used to perform proportional and non-proportional loading paths. Their design is calculated with an elastic behavior and the damage post-processor DAMAGE2005 so that potential cracks start in the *centre* of the gauge zone. The meniscus of zone is left rough milled with a roughness Ra ~ 0.4 m.

1.3 Loading and testing machine

The triaxial testing machine ASTREE ([7]) of the LMT-Cachan laboratory is used. The specimens are loaded by the 4 horizontal actuators (100 KN load capacity, 250 mm stroke range) at a frequency of 10 Hz. Several tests with cyclic loadings have already been performed on cross specimens with this machine ([8]): they are similar to Low Cycles or High Cycles Fatigue tests in terms of strain amplitudes, nonetheless the applied number of cycles is always below 10^5. The digital controller

(Instron 8800) allows each actuator to be controlled independently or in centroid control. The centroid control mode uses a relationship between two actuators along the same load axis to maintain the centre of the specimen motionless. The digital controller enforces "balanced forces" control by using special algorithms to operate the valve driver of each actuator (Figure 1 b). For each axis pair (solid lines actuators or dotted ones in Figure 1 b), the controller uses the sum and the difference of the forces along the considered axis. This "modal force" control has been used in all the biaxial tests presented hereafter. For each test, the cyclic loading is periodically stopped (usually every $5x10^3$, $10x10^3$ or $20x10^3$ cycles) to acquire images from the gauge zone at maximum and zero load.

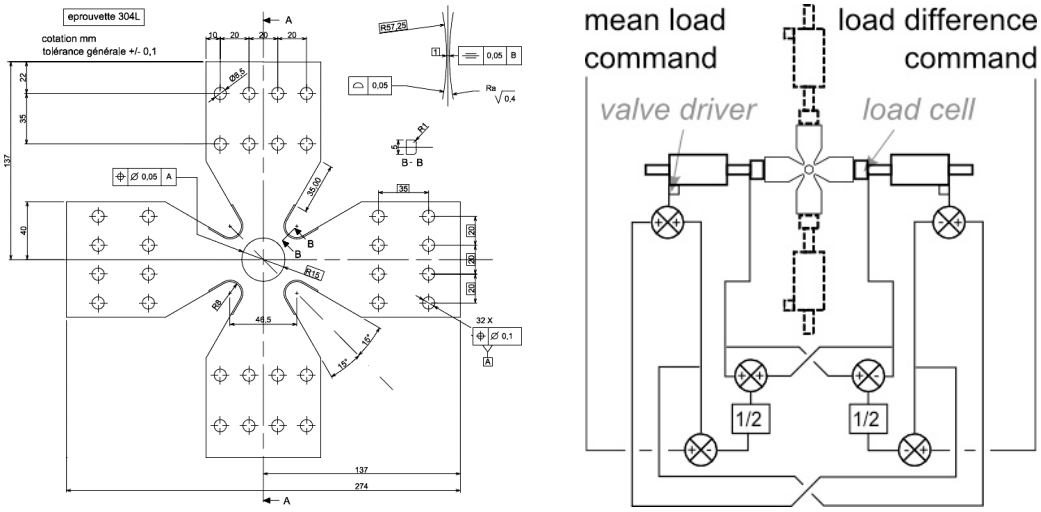

Fig. 1. (a) Specimens design; (b) "Modal force" control principle

1.4 Measurement devices

Some of the tests having a loading ratio about 0, a severe ratchetting phenomenon occurs which unables the use of strain gauge. It is thus proposed to measure strains in the gauge zone by use of Digital Image Correlation (DIC). One side of the specimens is consequently painted with a black and white speckle.

In order to minimize the strain measurement uncertainty, a CCD camera (PCO, Pixelfly, 1360 x 1024 pixels, 12 bits) with a telecentric lens x1 (Edmunds Optique) is dedicated to the strain measurement at the centre of the gauge zone. The Digital Image Correlation (DIC) is performed using the Correli-Q4 software [9]. The chosen Zone Of Interest (ZOI) is 480 x 480 pixels, *i.e.* a 3 x 3 mm² zone in the centre of the specimen. The average (uniform) strain in this zone is calculated with an uncertainty less than $2x10^{-5}$ in the real test conditions. A stroboscopic acquisition is performed to measure the strain over a cycle at the loading frequency (10 Hz) without needing a high speed camera. The loading feedback period is measured with a LabView routine which then triggers the camera so that virtual duration between each image is a ratio of the period (in the present case, 1/20). It is then possible to reorder the images of the recorded "movie" into a virtual complete cycle. This type of acquisition is done at the beginning of each series of $5x10^3$, $10x10^3$ or $20x10^3$ cycles.

A second image acquisition is performed with a Digital Reflex Camera (EOS 350D, 3456 x 2304 pixels) and a macro lens (SIGMA 105mm F2,8 DG Macro EX). This device is only dedicated to the acquisition of images at zero and maximal load to analyse the strain field on the whole gauge zone. It thus enables the tracking of (potential) cracks out of the central zone measured by the stroboscopic set-up.

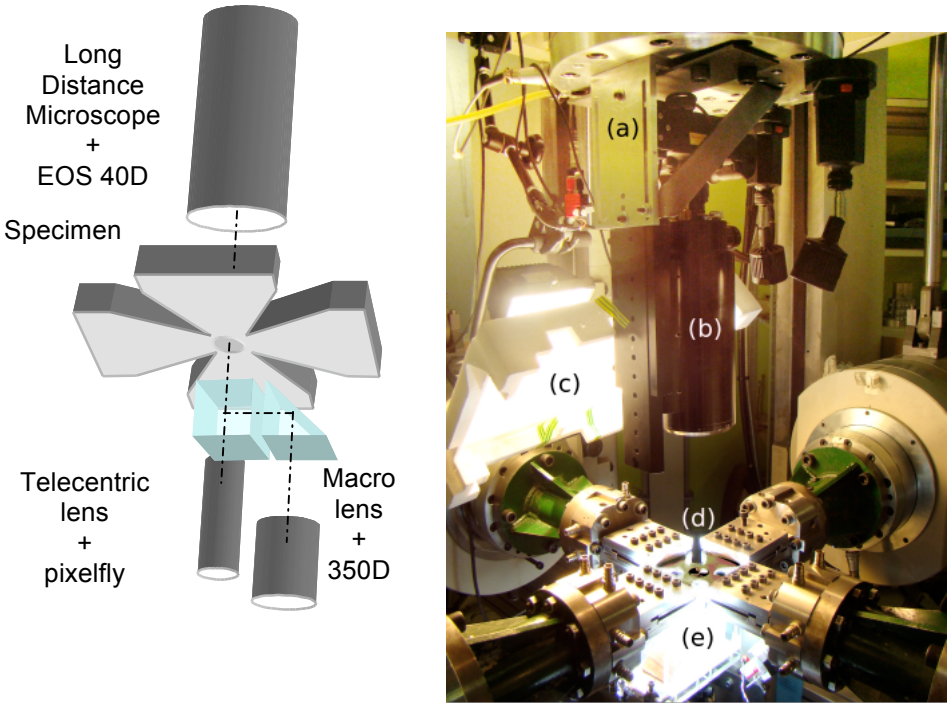

Fig. 2 (a) Optical set-up ; (b) Complete experimental set-up ([a] Digital single lens reflex, [b] Long distance microscope, [c] Diffuse lighting, [d] cross-specimen, [e] beam-splitter setup)

Both EOS 350D camera and Pixelfly camera shoot the same specimen face. They share the same optical axis because of a beam splitter (Figure 2 a). This is called "compound (parallel) strain measurement".

A last image recording device is placed on the opposite side of the specimen, whose face is not painted. It is composed of a digital reflex camera (EOS 40D, 3 888 x 2 592 pixels) and a Long Distance Microscope (LDM, Questar QM100, about x100 in the present conditions). The very short field depth (< 30 m) does not allow to acquire pictures at zero and maximal load (small out-of-plan displacement). Consequently only pictures at zero load are shot to detect crack initiation in the central zone (~ 2 x 2 mm²).

1.5 Loading paths

The different performed loading paths are summarized in Table 3. Three different loading paths are distinguished : proportional equibiaxial tests with positive loading ratio (ETT), negative loading ratio (ETC), and non-proportional tests with a cyclic loading in one direction and a constant one in the other. The number of tests performed so far for each loading path is also given. R_{F1} and R_{F2} are the force ratii in both directions.

ETT tests were the first ones to be conducted. Consequently the measurement protocol was not yet complete and validated for the first of them. This is the reason why some tests (ETT2 and ETT3) were repeated once the protocol was complete.

Table 3 : Definition of the loading paths

		Number of tests	F_1^{max}	F_2^{max}	R_{F1}	R_{F2}
Equibiaxial Tension-Tension (ETT)	ETT1	1	28 KN	28 KN	0.1	0.1
	ETT2	2	31 KN	31 KN	0.1	0.1
	ETT3	3	38 KN	38 KN	0.1	0.1
Equibiaxial Tension-Compression (ETC)	ETC1	1	19 KN	19 KN	-1	-1
	ETC2	1	21 KN	21 KN	-1	-1
Non-Proportional tension-tension with constant load (NP)	NP1	1	38 KN	0 KN	0.1	1
	NP3	1	38 KN	19 KN	0.1	1
	NP3	1	38 KN	38 KN	0.1	1

3 RESULTS AND DISCUSSION

Table 4 summarizes two examples of test results. The main measured load characteristics are presented (*i.e.* maximum force F^{max} and load ratio R_F for each axis), as well as the amplitude of strain $\Delta\varepsilon/2$ at half-lifetime and the residual strain $\varepsilon_{res}(N_t)$ at the number of cycles to initiation. The variation of amplitude with the number of cycles is low, so that for most of the specimens the strain amplitude at half-lifetime is a meaningful characteristic of the performed test. The shear strain amplitudes are not presented in the tables because they are negligible before crack initiation.

Table 4 : Example of tests results. The strain field shows the increment of residual strain during the last series of cycles, in the meniscus of the gauge zone. Depending on the crack orientation, ε_{xx} or ε_{yy} is plotted to better visualization. The circle stands for the gauge zone limit. The strain scale is the same for the two tests and the gauge diameter (black circle) is 30mm.

TEST	Axis	F^{max} (kN)	R_F	$\Delta\varepsilon/2$ (%)	$\varepsilon_{res}(N_t)$ (%)	N_i	Strain field at N_i (0.02 0.01 0 -0.01)
ETT2	x	31.0	0.07	0.077	1.700	no initiation after 10^6 cycles	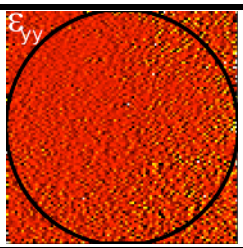
	y	31.0	0.08	0.075	1.566		
ETT3	x	38.0	0.10	0.100	6.145	[105000 ; 115000]	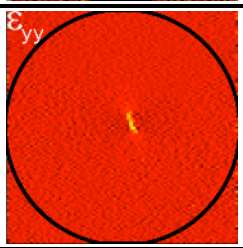
	y	38.0	0.10	0.099	5.021		

An equivalent strain is chosen to compare the obtained results to uniaxial ones. To prove that the presented results do not depend much of the chosen equivalent strain, two different equivalent strains are chosen, namely the maximum strain amplitude and the von Mises equivalent strain amplitude. For the sake of brevity the calculus of these strains is not presented here. It is only worth noting that the value of the equivalent amplitude depends on the assumption of elasticity or (pure) plasticity, so that results have to be plotted within a range for each equivalent amplitude, symbolized by a vertical line between each pair of values.

Figure 3 gathers all the currently available fatigue results and some uniaxial ones [6] obtained for imposed strain amplitude (same 304L material). Every crack initiation occurs in the *centre* of the gauge section and was early detected by the strain field measurement as shown Table 4. The error bars plotted on the uniaxial results also represent range due to elastic or plastic assumption.

Several points have to be noted :

- No conclusions must be drawn up to now from Figure 3 (a) and (b) concerning biaxiality effect. First because only two loading paths were tested, both leading to no failure. Second because the size effect is not yet taken into account (uniaxial specimen geometry and biaxial one are very different). Rough estimation of this size effect leads nonetheless seemingly to a minor biaxiality effect. Furthermore, considering[b] NP1 test as a uniaxial test performed on the same biaxial geometry, one remarks that NP1 plot is approximately on the same Whöler curve as the ETT tests, which also suggests that biaixiality effect is low for tests with R_f=0.1.
- The mean stress effect for biaxial loadings is on the contrary clearly visible by comparison between ETT tests (R=0.1) and ETC ones (R=-1).
- Last, the effect of a constant load perpendicular to a cyclic one (*i.e.* non-proportional loading path with constant load) is tremendous (figure 3 (e) and (f)).

This last series of non-proportional tests is the subject of an in-depth study for several reasons. A particular crack "network" appears on the specimen NP3, where only one large fatigue crack is found (opened by the cyclic loading) but numerous perpendicular cracks (usually without any striae). Moreover the residual strains due to ratcheting (figure 4) show a "competition" between the direction of cyclic loading (F_1) and constant loading (F_2). In case of high constant load, the strain in this second direction is dominant, whereas it is the opposite for low constant load.

4 CONCLUSION

An experimental protocol including strain field measurements and micrographic observations has been developed to accumulate the maximum of information on each test of a multiaxial HCF campaign. It allows the accurate measurement of strains under cyclic loading in the centre of the gauge zone as well as crack initiation detection on the whole gauge zone.

Up to now the effect of the mean stress on biaxial loading turns out to be important, as well as the effect of a constant load applied perpendicularly to a cyclic load.

Several tests are to be performed to complete current ones and better understand damage evolution (equibiaxial R=-1 tests, non-proportional tests with high micrographic magnification, cyclic behavior tests, random loading, etc.). Numerical simulations will link the applied load and the real loading in the *centre* of the gauge zone. Micrographs and statistical analysis of the crack population will also complete this study. All these results help in the validation of the damage post-processor DAMAGE.

[b] This test with constant load set to zero is not stricto sensu a uniaxial test because of structural effect. Strain measurements show however that it is close to a pure uniaxial one.

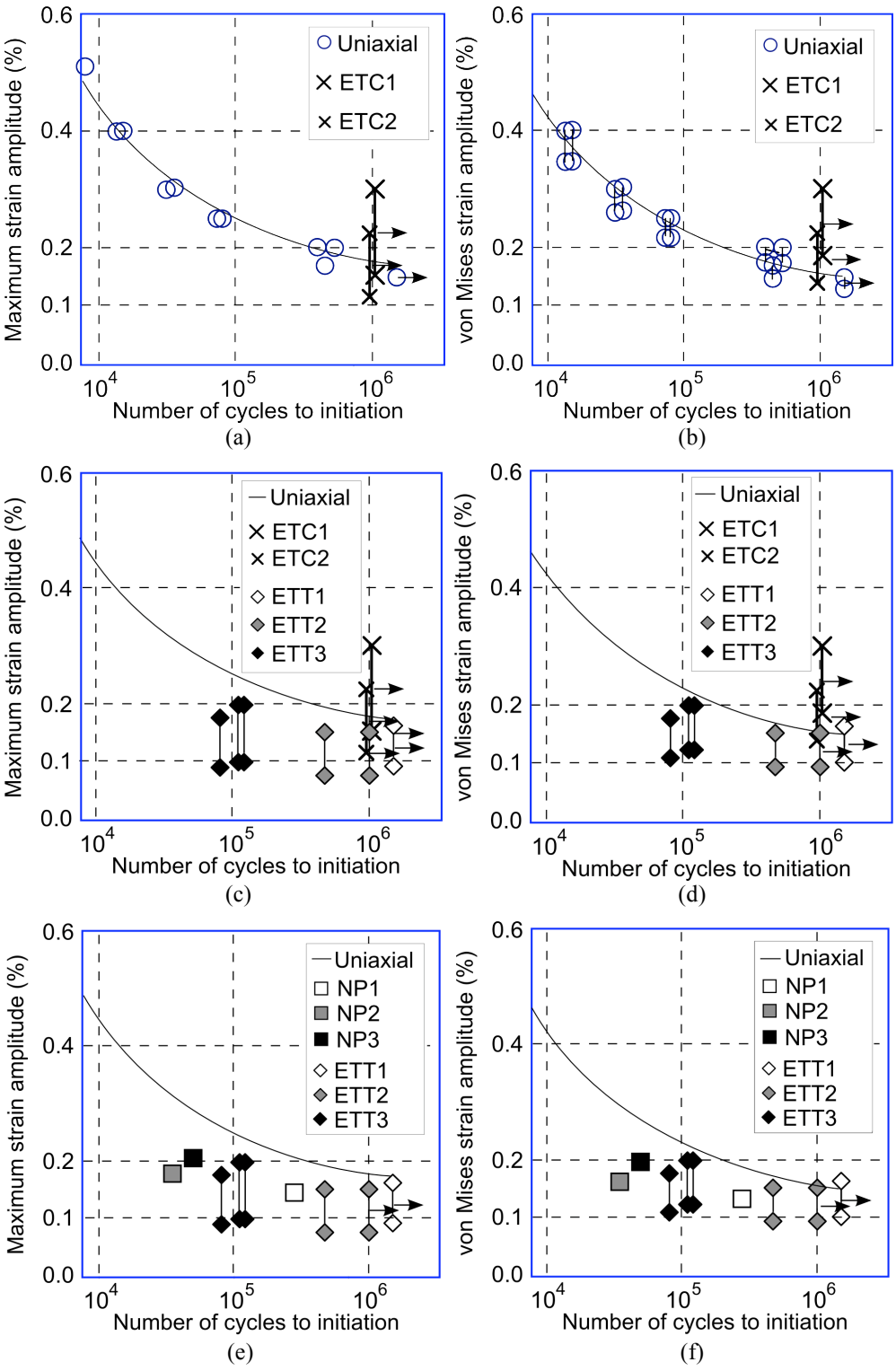

Fig. 3 Manson-Coffin curves plotted with maximum and von Mises equivalent strain amplitudes : (a,b) effect of biaxiality; (c,d) effect of load ratio; (e,f) effect of non-proportionality. Solid line curves stand for the mean curve of the uniaxial results.

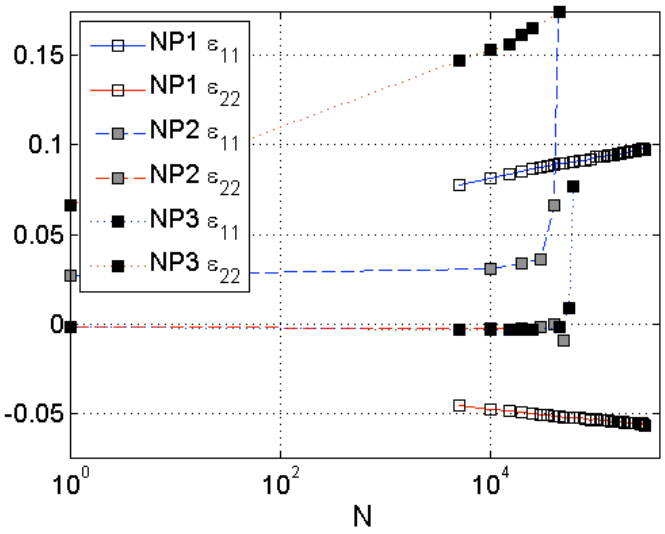

Fig. 4 Evolution of the residual strain during the different tests of the non-proportional tests series.

References

1. J.-M. Stephan, F. Curtit, C. Vindeirinho, S. Taheri, M. Akamatsu, C. Peniguel, Evaluation of the risk of damage in mixing zones: EDF R & D programme. *Fatigue 2002*, 1707–1714 (2002)
2. V. Maillot, Amorçage et propagation de réseaux de fissures de fatigue thermique dans un acier inoxydable austénitique de type X2CrNi18-09 (AISI 304 L), PhD thesis, Ecole Centrale de Lille (2003)
3. N. Haddar, Fatigue thermique d'un acier inoxydable austénitique 304L : simulation de l'amorçage et de la croissance des fissures courtes en fatigue isotherme et anisotherme. PhD Thesis, ENSMP (2003)
4. R. Desmorat, A. Kane, M. Seyedi, J.-P. Sermage, Two scale damage model and related numerical issues for thermo-mechanical High Cycle Fatigue, European Journal of Mechanics - A/Solids, **26**, 909–935 (2007)
5. P. Delobelle, P. Robinet, L. Bocher, Experimental study and phenomenological modelization of ratchet under uniaxial and biaxial loading on an austenitic stainless steel, Int. J. Plasticity, **11**, 295–330 (1995)
6. J.-C. Le Roux, Influence de paramètres métallurgiques et d'essai sur l'amorçage des fissures de fatigue en déformation imposée des aciers inoxydables austénitiques, Projet t2-00-04 (domzone), Note EDF R&D HT-26/03/056/B (2004)
7. S. Calloch and D. Marquis, Triaxial tension–compression tests for multiaxial cyclic plasticity, Int. Jal of Plasticity, **15(5)**, 521-549 (1999)
8. C. Doudard, M. Poncelet, S. Calloch, C. Boue, F. Hild, A. Galtier, Determination of an HCF criterion by thermal measurements under biaxial cyclic loading. Int Jal of Fatig., **29(4)** 748-757 (2007)
9. G. Besnard, F. Hild, and S. Roux. "Finite-element" displacement fields analysis from digital images: application to Portevin-Le-Châtelier bands. Exp. Mech., **46(6)**, 789–804 (2006)